ORIGINAL PAPER

Power quality assessment and compliance of grid-connected PV systems in low voltage networks using microinverters

D. Atsu[1,4] · I. Seres[2] · I. Farkas[3]

Abstract

Solar PV has experienced unprecedented growth in the last decade, with the most significant additions being utility-scale solar PV. The role of grid inverters is very critical in feeding power from distributed sources into the grid. With the increasing growth of grid-tied solar PV systems (both rooftop and large-scale), the awareness of power quality issues has risen with new regulations and standards to ensure the stability of the power grid. The power quality of microinverters has been investigated under steady solar irradiation and PV power source and also under real outdoor conditions in compliance with the accepted solar PV integration requirements. The current total harmonic distortion (THD) measured for the studied microinverter under outdoor conditions far exceeded the current THD for the study under steady indoor conditions and was beyond the accepted standard. However, the voltage THD outputs for the two studied cases were in good agreement with the grid codes. The voltage and current THD for the 400 Wm^{-2} (60 Wp) and the 1000 Wm^{-2} (146 Wp) scenarios under the steady solar irradiation (solar PV power) were 2.24%, 13%, and 2.27, 6.93%, respectively. The voltage and current THDs for the outdoor study were 2.03% and 14.28% for Solarex (pc-Si module), 1.94%, and 27.43% for Juta (mc-Si modules), and 1.97% and 33.6% for Dunasolar (a-Si glass module). Results showed a strong correlation between the intermittence of solar radiation and the current THD. 67%, 54%, and 37% of the recorded power factor for Dunasolar, Juta, and Solarex modules, respectively, exceeded the limits prescribed by the standards.

✉ I. Farkas
farkas.istvan@uni-mate.hu

1 Doctoral School of Mechanical Engineering, Hungarian University of Agriculture and Life Sciences, Gödöllő, Hungary

2 Institute of Mathematics and Basic Sciences, Hungarian University of Agriculture and Life Sciences, Gödöllő, Hungary

3 Institute of Technology, Hungarian University of Agriculture and Life Sciences, Gödöllő, Hungary

4 Department of Energy Systems Engineering, Koforidua Technical University, Koforidua, Ghana

🙋 Springer

1 Introduction

Integration of distributed generated (DG) systems into the utility portfolio has several benefits in enhancing the power quality by reducing power losses and improving the voltage profile and stability [1]. However, just integrating DG does not guarantee the benefits of enhancing the power quality of the grid, but the proper siting [2] and the type of conversion components employed play a major role.

In recent years, various countries, and regional organizations have prioritized the exploitation of distributed energy sources due to their numerous benefits [3, 4]. Consequently, the power quality issues have increased in recent years as more distributed energy sources that employ vast electronics in their composition are being integrated into the utility grid. The increasing use of non-linear loads in the wake of modernization is another source of power quality (harmonic) issues. These non-linear loads may include computers and other electronic accessories, ballasts, power supplies, motors, and LED bulbs. Linear loads do not introduce power quality issues in the grid because they withdraw current at the same frequency as the voltage. This is, however, not the same for non-linear loads. They draw currents at different frequencies to that of the voltage; thus, obtaining non-sinusoidal currents. The extent of the waveform distortion is dependent on the type or nature of the non-linear load and its interactivity with other units in the network leading to the distortion of the grid power supply [5].

With the introduction of several national and regional policies for the adaptation and utilization of solar PV, different types of models and schemes at various scales are being applied by various governments and private organizations to meet the requirements of different consumers. The recent introduction is the microinverter unit. This type of inverter can be employed as a standalone unit, which is usually installed close to the load or (grid meter) to generate AC power using mainly one or two modules that are connected to meet the low input voltage of the microinverter. The microinverter offers the opportunity to monitor the performance of each module, making troubleshooting straightforward to undertake.

Microinverters are usually applied to systems with nominal power ranging from 200 Wp to about 600 Wp and are incorporated with maximum power point trackers (MPPT) for stable operation. One advantage of microinverters is that they generate less internal temperatures and also, their constitution is devoid of bulky electrolytic capacitors for input power decoupling. These make them have an average lifespan of 25 years, regardless of the weather conditions [6]. Studies have shown the advantages of microinverters have over the string inverters [7]. The fact that each module has a dedicated MPPT, module mismatch is eliminated, and there is also the minimal occurrence of shading, which is a common issue with residential or rooftop PV systems [8]. Microinverters also possess the edge of being compact, with low maintenance requirements, and are easy to install and operate hence the gain in attention in recent years.

Microinverters are composed of either the single-stage with the implementation of the maximum power point tracker or the double-stage conversion topology, which makes use of the DC-to-DC converter in the absence of MPPTs [6]. To further enhance the acceptance and dissemination of microinverters, they are constructed less bucky and easy to self-install with signal outputs close to the grid [9, 10].

Galvanic isolation is required in interfacing the inverter with the grid to help resolve the problem of grounding [10]. The presence of the galvanic isolation determines the essence of a transformer in the inverter. This is because the galvanic isolation is obtained with the company of the transformer. Usually, in the case of the availability of a transformer in the microinverter, they are situated at the DC side with a high-frequency operation because of their small sizes. It has been found that microinverters without transformers improve efficiency by 2% and enhance the power density [11, 12]. However, there is also the fear of high content of leakage current [13], which occurs due to stray capacitance that exists between the module terminal and the ground. High leakage current could have a significant effect on the output power of the PV system and its reliability if it is not resolved by using the right means such as adding switches or acting on the pulse width modulation or applying passive filters [14]. These parasitic capacitances can reach as high as 150 µF/kWp or 1 µF/kWp for crystalline silicon cells and amorphous silicon cells, respectively, and depend on the temperature and other climatic factors present at the site [15]. Studies have shown that stray current could be bypassed by creating an alternative conducting channel without incorporating more switches into the microinverter [16].

Several researchers have listed many microinverters having power output ranging from 90 to 600 Wp with power density ranging from 0.09 to 0.41 W/cm^2. The listed microinverters possess maximum power point voltage ranging between 15 and 37.8 V while the power factor and total harmonic distortion range from 0.95 to 1 and $\leq 2.9\%$ to $\leq 5\%$, respectively [13, 17].

Different designs of microinverters have been propounded in various studies and are in operation. However, regardless of the topology of the microinverter, technically, it is made up of the following units: the DC-DC converter, the inverter, the control unit, a protection circuit, and an interface that links it with the grid. A typical outlook of a microinverter with the essential components is shown in Fig. 1 [18].

A study by [19] on the thermal performance of micro inverters revealed a strong correlation between the degree of the temperature of the microinverter with irradiation, the temperature of the PV module, the temperature of the surrounding, and the nominal AC power out of the module. This study investigates the performance of microinverters under a steady irradiation source (solar PV simulator) and also under outdoor ambient conditions. The power quality characteristic measurements for different scenarios will be analyzed and results compared with other studies on microinverters as well as compliance with available standards for grid-connected PV systems.

The contribution of this paper consists of the presentation of the effects of different operating conditions on the performance and efficiency of the output of microinverters in a stable load-free grid subsystem. The power quality characteristics for various scenarios for the microinverters are analyzed and results are presented
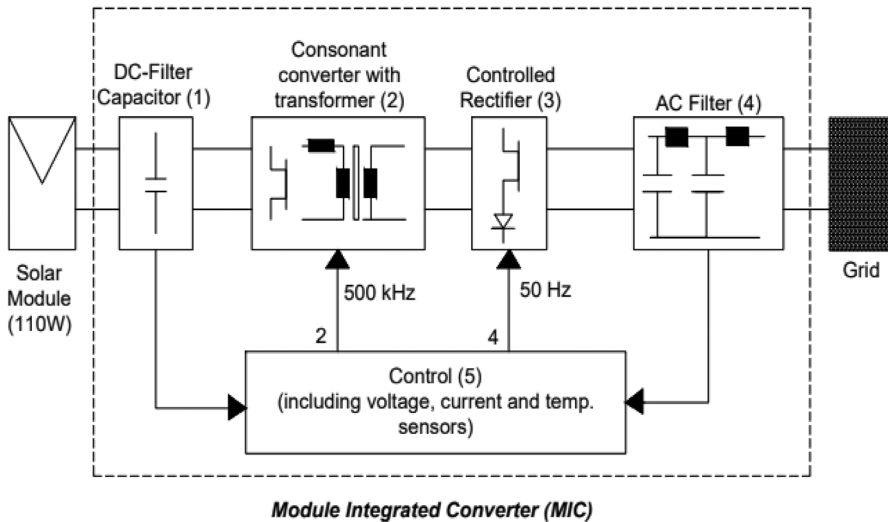
Fig. 1 A classic example of a microinverter [18]

vis-a-vis their conformance with acceptable standards for grid-connected PV systems.

The remaining part of the paper is organised as follows: Sect. 2 presents the materials and the description of the methods employed in the study. In Sect. 3, the measured data is discussed and analyzed, comparing the results of each setup and scenario and also assessing the compliance with known standards observed in the sub-region of the experimental study. In Sect. 4, the conclusions of the paper are presented.

2 Materials and methods

The compactness of microinverters enables their easy fixation at the back of PV modules. The primary role of microinverters is to extract the maximum power of a module and inject the AC component into the grid while meeting the standards set by the utility regulators for grid-connected PV systems. This section describes the different materials, methods, and locations for the acquisition of data.

2.1 Measurements with the solar PV simulator

The study was to analyze the quality of the power output of the microinverter by employing different modules of different technology and make (structure) that meet the requirements of the inverter. The Geräte Unterricht Naturwissenschaft Technik (GUNT) ET255 set-up has been retrofitted to conduct the experiment, as described below. The setup is made up of a photovoltaic simulator, connecting sockets for solar photovoltaic modules, and a toggle switch to change between either operating the

Table 1 Characteristics of module inverter

Parameter	Value
Maximum input power	150 W
Grid feed-in from	2.5 W
Maximum input voltage	55 V
Output voltage	230 V
Switch-on voltage	35 V

Table 2 Characteristics of PV generator

Parameter	Value
Power output	150 W
Current at maximum output	4.7 A
Voltage maximum output	31.4 V
Maximum short circuit current	5.1 A
Maximum open circuit voltage	41.3 V

photovoltaic simulator or the photovoltaic modules. A combiner box with terminals for the integration of extra PV module strings depending on the size of the PV system. The combiner box contains an overvoltage protection system to safeguard the components of the setup. The setup has the DC switch disconnector, which isolates the PV generator from the other parts should a failure occur. The voltage and the current limits of the DC switch disconnector are set at the maximum Voc and Isc values of the PV generators and PV simulator. The grid-connected inverter employed is a micro-inverter (module inverter) designed for small outputs of about 200 W. It has an in-built maximum power point tracking (MPPT) function. The switch-on voltage of the inverter is 35 V, and the MPP voltage tracking range lies between 28 and 50 V. The specifications of the module inverter are presented in Table 1. The GUNT ET255 was retrofitted with measurement points to enable the measurement of AC voltage and current simultaneously and evaluate the power quality characteristics of the various waveforms generated under the different scenarios.

The first test was conducted using the PV simulator as the source of PV power to feed the inverter. Two scenarios were considered as constant irradiation and module temperature at 1000 Wm^{-2} and 25 °C, respectively. This selection generates a steady nominal power of 146 Wp, Voc of 41.3 V, Isc equals 5 A, Vmpp of 31.4 V, and Impp 4.65 A. The second scenario with the PV simulator as the source of the PV power, employed irradiation of 400 Wm^{-2} at a constant module temperature of 25 °C, generating Voc of 39.6 V, Isc 2 A, Vmpp 32.3 V and Impp 1.87 A. These two conditions are to assess the system quality performance at the two extreme states under steady irradiation and PV power as presented in Table 2).

The second investigation with the GUNT ET 255 employed PV modules in real outdoor operation as the source of the DC power. In this case, different technologies and structures of PV modules were used to assess the quality of the power output of the system/microinverter.
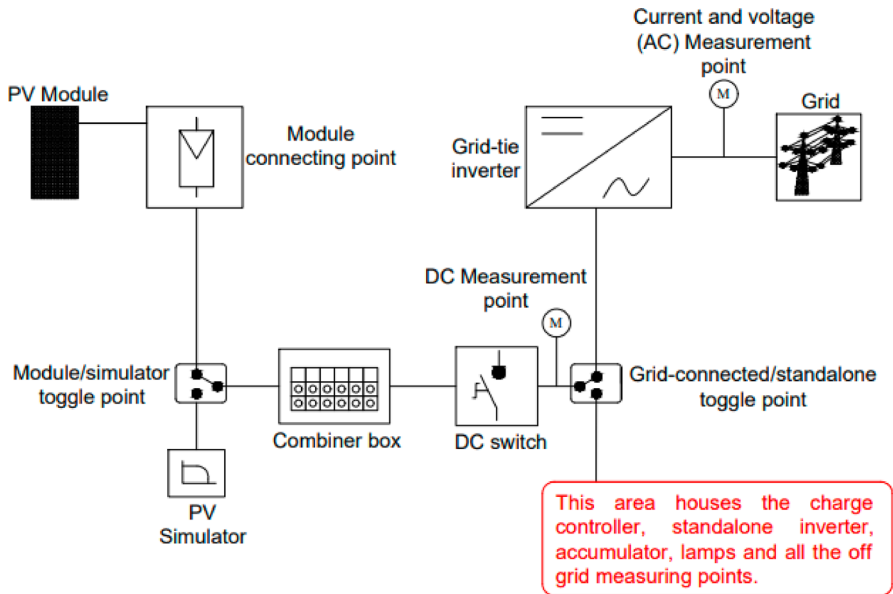
Fig. 2 Schematic diagram of the setup

Fig. 3 Experimental setup

In order to measure both AC current and AC voltage output simultaneously and to obtain the power quality characteristics of the inverter output, additional measurement points have been created on the ET 255 for connection to the power analyzer. The schematic diagram and the image of the setup are shown in Figs. 2 and 3, respectively. Measurements were done for a duration of 8 h.

The Wally A3 electric power quality analyzer with an in-built logging capability was used to measure and store the characteristics of the AC output waveform. Table 3 presents the specifications of the Wally A3 analyzer.

Table 3 Specifications of Wally A3 power analyzer

Ranges	Voltage	0–400 Vac
		0–100 Vac
	Current	5 Arms (direct insertion)
		3 Vac/dc (from current clamps with voltage)
		3KA/300 A (from flexible clamps Rogowski)
	Frequency	DC or 42.5–69 Hz
Accuracy	Voltage	$\pm 0.1\%$ U_{din} from 10 to 150% of U_{din}
	Current	$\pm 0.1\%$ I_{din} from 10 to 150% of I_{din}
	Frequency	± 10 mHz
	Harmonics	Meet EN 61000-4-7 class 1
	Flicker	Meet EN 61000-4-15
	Power quality	Meet EN 61000-4-30 Class A

The measurements are computed over 10–12 cycles of consecutive windows, according to IEC 61000-4-30. Sampling is done synchronously with phase-locking at 512 samples/cycle with a range of 42.5–69 Hz (25.6 kHz @ 50 Hz).

Solar radiation data was measured at the plane of the module or array (PoA) using the Delta-T SPN1 Pyranometer with specifications presented in Table 4. The ADAMS 4018 interface is used to extract the measured irradiation and then converted into a digital signal and stored in the computer.

The Almemo 2290-4 multimeter with a data logger option was used to acquire the ambient temperature and the temperature of the rear of the modules. A measuring module NiCr-Ni (K), Pt 1000, with the range -200.0 to $+1370.0$ °C having a resolution of 0.1 K was used. Temperature sensors (resistance temperature detector, RTD) 1 kΩ Platinum (Pt 1000) with accuracy $\pm 0.001\%$, ± 3850 ppm/°C, 2-SIP was applied for the temperature measurement.

2.2 Data curation on PV modules in real operation

The study was undertaken at the forecourt of the Solar Energy Laboratory at the Hungarian University of Agriculture and Life Sciences, Gödöllő, Hungary, which has geographical coordinates of 47° 35′ 39″ N, 19° 22′ 0″ E. The modules used for the research have no particular predefined criteria for selection, but available modules which have two distinct makes and structure were used. The two main

Table 4 Specifications of the Delta-T SPN1 Pyranometer

Accuracy	± 0.1 W/m
Spectral sensitivity	400–2700 nm in W/m^2
Resolution	1 W/cm^2
Signal output	0–2 V
Linearity	$< 1\%$
Temperature coefficient	$\pm 0.02\%$/°C

Table 5 Module characteristics at standard test conditions (STC)

	DUNA SOLAR	SOLAREX	JUTA
Parameter	a-Si (G-G)	pc-Si (G-T) (60Wp)	mc-Si
P_{mpp} (W$_p$)	40	60	20
V_{oc} (V)	62.5	21.3	22
I_{sc} (A)	1.15	3.8	
V_{mpp} (V)	44.0	17.1	17
I_{mpp} (A)	0.90	3.5	1.18
Module Area/ (m^2)	0.791	0.564	0.36
Temp. coeff. of power	− 0.47%/C	− 0.47%/°C	− 0.4%/°C
Stratigraphy	Glass-EVA-CELL-EVA-Glass (No frame) (G-G)	Glass-EVA-CELL-EVA-Tedlar (With frame) (G-T)	Glass-EVA-CELL-EVA-Tedlar (With frame) (G-T)

Fig. 4 Installation of PV modules

technologies used are glass-cell-glass structure and glass-cell-Tedlar structure. The modules are the Dunasolar, Solarex, and Juta modules. The variety of the module assembly allows for the comparison of the power quality of the technologies. Module specifications, as given by the manufacturer, are presented in Table 5. Modules are fixed to an inclined support facing true south and having an angle to the horizontal equal to the site's latitude. The installation of the modules is shown in Fig. 4. In order that the modules voltage output meets the kick-start voltage of the microinverters, the experiments are conducted on bright sunny days. Measurements for each scenario were taken for 10 h (8 am–6 pm) in the second week of August 2020.

2.3 Mathematical methods

The following methods and formulas were employed in computing the characteristics of the AC waveform output are as follows:

Flicker (EN61000-4-15)—Short term flicker

$$P_{sti} = \sqrt{0.0314P_{0.1} + 0.0525P_{1s} + 0.0657P_{3s} + 0.28P_{10s} + 0.08P_{50s}} \tag{1}$$

P = flicker levels exceeded for tt% where (tt = 0.1; 1; 3; 10 e 50) of the time for the observation.

Flicker (EN61000-4-15)—Long term flicker

$$P_{lt_i} = \frac{\sqrt[3]{\sum_{i=1}^{N} P_{st_i}^3}}{N} \tag{2}$$

N = 12, i = 1,2,3

THD

$$THD_{1i} = \sqrt{\sum_{h=2}^{50} \left(\frac{Y_{sg.h_i}}{Y_{C,1_i}}\right)^2} \tag{3}$$

Y_{sg,h_i} = harmonic order of h, where i = 1,2,3.

CosΦ

$$Cos\Phi_{Li} = \frac{W_{Li}}{\sqrt{W_{Li}^2 + Q_{Li}^2}} \tag{4}$$

i = 1,2,3

Harmonic order n (thus the harmonic subgroup as per EN61000-4-7 are computed over 10–12 cycles window)

$$Y_{sg,h} = \sqrt{\sum_{k=-1}^{1} Y_{C,h+k_i}^2}$$

$Y_{C,hi}$ = spectral component of order $h_{th,}$ h = 0–50, i = 1,2,3.

3 Results and discussion

The growth of solar PV has been so quick and has overgrown what the development of grid codes could cope with. As a result, there are relatively different grid connection specifications for various countries. There are diverse views as to whether PV systems should be passive or perform actively in grid control. Therefore, there is the need for the harmonization of codes taking into account the robustness of the various power networks [20]. Several proposals of microinverter topology have been made which are basically composed of either the single-stage with the implementation of the maximum power point tracker or the double-stage conversion topology. Single-stage microinverters make use
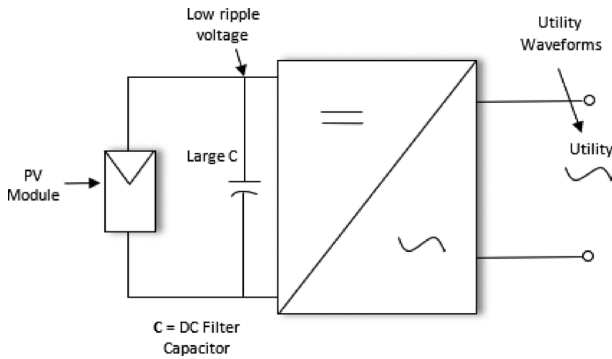
Fig. 5 Single-stage microinverter
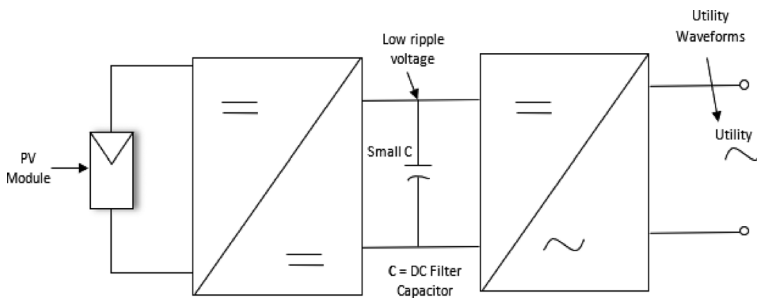
Fig. 6 Double-stage microinverter [2]

of a large capacitor for energy storage at the PV side of the converter (Fig. 5). The capacitor mostly used for this purpose is the electrolytic capacity which has reliability issues [1]. The two-stage microinverter achieves higher reliability by using a DC-DC converter at the PV side which feeds the DC-link capacitor with the extracted power [2]. The DC-DC converter at the PV side is able to extract the maximum power from the PV module. In the two-stage approach, a non-electrolytic capacitor is applied and medium to high ripple voltage can be tolerated at the DC-AC link, unlike the single-stage topology where only a low ripple voltage is tolerated at the PV module side of the converter. The second phase of the conversion process in the two-stage topology can be made up of either a PWM inverter or a low-frequency circuit as shown in Fig. 6 [2]. Both single-stage and double-stage microinverters can have transformers incorporated in them to perform the role of islanding.

In this section, the measured data is analyzed, comparing the results of each setup and scenario and also assessing the compliance with known standards observed in the subregion of the experimental study.

3.1 Results of the measurements with the solar PV simulator

In this subsection, the results obtained from the measurements on the solar PV simulator are discussed, taking into account the various standards for grid-connected systems.

3.1.1 Voltage profiles during the use of the solar simulator

Figure 7 presents the voltage profiles of both scenarios for the solar simulator with the microinverter. Voltage measurements were done at 200 ms intervals. The voltage output for the 400 Wm^{-2} recorded maximum and minimum values of 240.8 V and 230. 3 V, respectively, during the period of the experiment. The mean voltage and the standard deviations were 236.3 V and 1.9934 V, respectively. It was noticed that there were no dips during the period as all voltages were above the nominal voltage of 230 V. The recorded voltages were all in the standard operating range as prescribed by the EMC standards, EN 50160, EN 61000 as $\pm 10\%$ for low voltage and medium voltage power systems [21]. On the other hand, the voltage profile for the 1000 Wm^{-2} recorded some values below the nominal voltage, even though they were minimal (less than 0.5%). The average voltage and the standard deviations were 235.9 V and 1.545 V, respectively. The range of disparity is about 10 V. The high standard deviation value for the 400 Wm^{-2} shows the high disparity in its recorded voltages compared to the values recorded for the 1000 Wm^{-2}. It is observed that during two-thirds of the period of the measurement, the voltage of the 400 Wm^{-2} was higher than the figures for the 1000 Wm^{-2}, except in the middle one-third, where the values for both scenarios had minimal differences.

The voltage deviations show the same trend as the profile of the voltages of the two scenarios. The 400 Wm^{-2} showed higher positive deviations during the early stage and later stages of the measurement, as shown in Fig. 8. The highest voltage deviation of 4.712 V was recorded by the 400 Wm^{-2}.
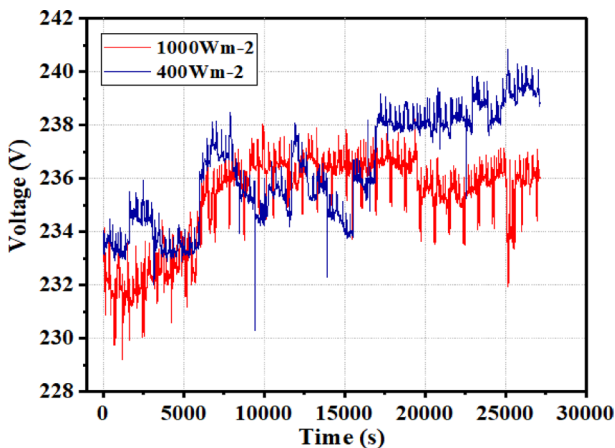

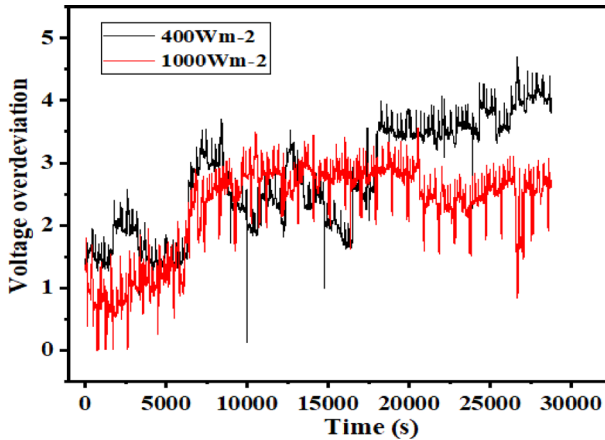**Fig. 7** Voltage profile when the solar simulator is applied (400 Wm^{-2} and 1000 Wm^{-2})

Fig. 8 Voltage deviations when the solar simulator was used (400 Wm^{-2} and 1000 Wm^{-2})

3.1.2 Voltage flickers

Due to the varying nature of solar irradiation, the penetration of solar PV systems in the grid can cause voltage flickers to occur. Voltage flickers are assessed based on the frequency of occurrence and deviation from the nominal voltage over a stated period according to the IEEE 1453 standard. To enable the proper management of voltage flickers, they have been classified as short-term probability flicker severity (Pst) and long-term probability flicker severity (Plt). The occurrence of flickers is observed in the sudden changes in the brightness of lamps with the noticeable flicking of the lights [22]. According to lower voltage characteristics, the EMC standard of EN 6100 prescribes Pst < 1.0 and Plt < 0.8. The IEEE 1547, and IEC 61000-3-3 standards also require that voltage flickers be between 0.6 and 0.9 pu for Plt and Pst, respectively [23]. The measured short-term voltage flickers for 400 Wm^{-2} and 1000 Wm^{-2} scenarios are presented in Figs. 9 and 10. Voltage flickers were recorded at the intervals of 3 s. There were no Plt flickers registered for any of the test scenarios with the solar simulator. The 400 Wm^{-2} had higher magnitude flickers compared to the 1000 Wm^{-2}. The highest and minimum flickers recorded were 2.248 and 0.1 and 1.552 and 0.088 for 400 Wm^{-2} and 1000 Wm^{-2}, respectively. 15.5% of the recorded flickers for 400 Wm^{-2} were outside the standard range while it was 5% for the 1000 Wm^{-2}. This, therefore, indicates a comparably higher level of quality issues under low irradiation conditions even under a constant source using the solar simulator.

3.1.3 Harmonic distortion

Harmonic distortions have been measured for both 400 Wm^{-2} and 1000 Wm^{-2} scenarios, and the results are shown in Figs. 11 and 12, respectively. The presence of harmonics in power systems distorts the AC current and voltage waveforms. The awareness of harmonic distortions in power systems has increased in recent years
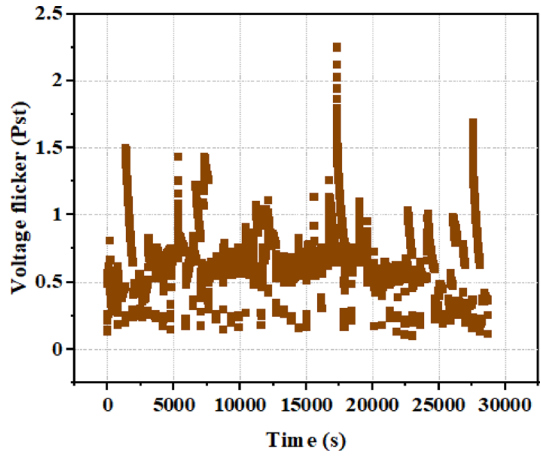
Fig. 9 Flicker—Pst (400 Wm^{-2})
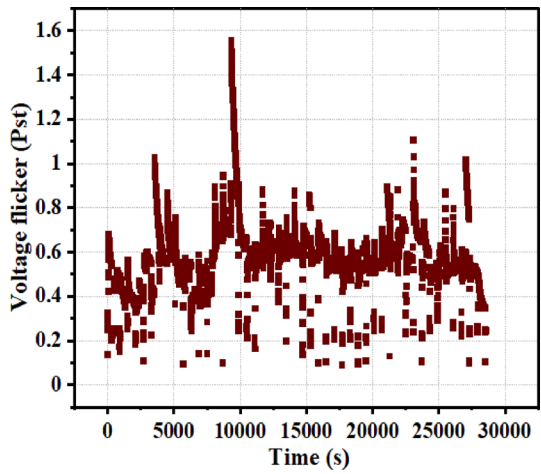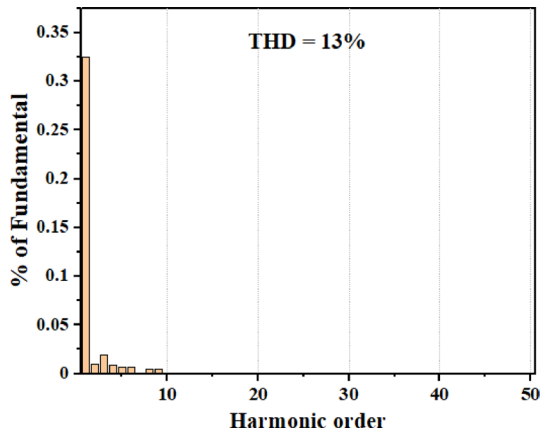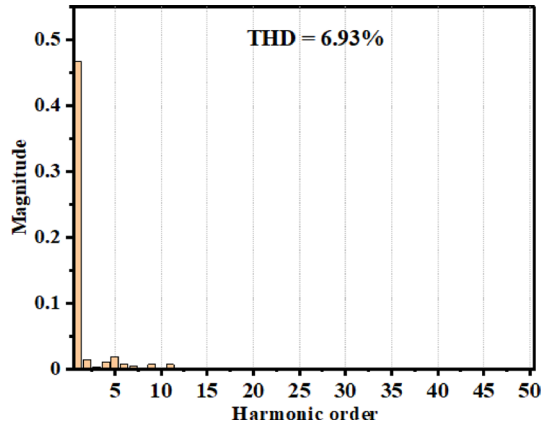

Fig. 10 Flicker—Pst (1000 Wm^{-2})

Fig. 11 Current harmonic for 400 Wm^{-2}

Fig. 12 Current Harmonics for 1000 Wm^{-2}

with the high penetration of distributed energy sources, especially with regard to variable sources. The use of grid inverters, which are mainly incorporated with power electronics, is the most significant source of harmonic distortion at the point of common coupling with the grid, consequently affecting the healthy performance of the grid and also causing the grid protection devices to malfunction. The limits for harmonic current emission as prescribed in the IEC 61000-3-2, IEEE 1547, AS 4777.2 standards are listed in Table 6 and the voltage harmonic standards are listed in Table 7.

Results show that the individual harmonic distortions of both 400 Wm^{-2} and 1000 Wm^{-2} scenarios were within the limit prescribed by the IEEE 519 and the IEC 61000-3-2 standards. The individual harmonic distortions for both scenarios were all below 0.5%. The highest for the 400 Wm^{-2} was 0.32% (1st harmonic) and 046% (1st harmonic) for the 1000 Wm^{-2} scenario. However, the total harmonic distortions

Table 6 Current harmonic distortion limits for grid-connected PV systems of some available standards and countries

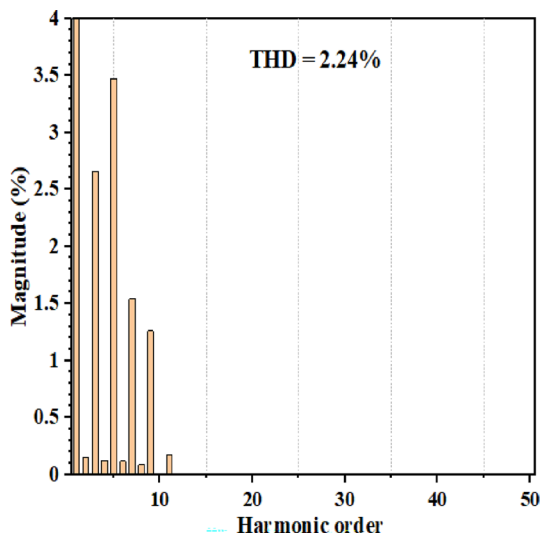| The standards	Type	Harmonic order (h)	Distortion limit	THD (%)
IEEE 1547 AS 4777.2	Odd	$33 < h$	$< 0.3\%$	$< 5\%$
		$23 \leq h \leq 33$	$< 0.6\%$	
		$17 \leq h \leq 21$	$< 1.5\%$	
		$11 \leq h \leq 15$	$< 2\%$	
		$3 \leq h \leq 9$	$< 4\%$	
	Even	$10 \leq h \leq 32$	$< 0.5\%$	
		$2 \leq h \leq 8$	$< 1\%$	
IEC 61000-3-2	Odd	$h = 3, 5$ and 7	$< (3.45, 1.71,$ and $1.15)$ %	$< 5\%$
		$h = 9, 11$ and 13	$< (0.6, 0.5,$ and $0.3)$ %	
		$15 \leq h \leq 39$	$< 0.225\%$	
	Even	$h = 2, 4$ and 6	$< (1.6, 0.65,$ and $0.45)$ %	
		$8 \leq h \leq 40$	$< 0.345\%$	

Table 7 Voltage harmonic distortion limits of PV systems

The standards	Voltage bus	Individual harmonics (max) (%)	THD (%)
IEEE 519	$(V \leq 1)$ kV	5	8
	$(1 \leq V \leq 69)$ kV	3	5
	$(69 \leq V \leq 161)$ kV	1.5	2.5
	$(V > 161)$ kV	1	1.5
IEC 61000-3-2	$(2.3 \leq V \leq 69)$ kV	3	5
	$(69 \leq V \leq 161)$ kV	1.5	2.5
	$(V > 161)$ kV	1	1.5

far exceeded the standard limit of 5%. The THD for 400 Wm^{-2} and 1000 Wm^{-2} were 13% and 6.93%, respectively. The THD decreased with increasing irradiation (high power) levels from the solar simulator. The extent of the harmonic content of the output signal is dependent on the carrier frequency and the switching function. In order to obtain an efficient output from the solar PV system, the operational range of the amplitude modulation index is usually fixed from 0.5 to 1.0 [24]. The harmonics decrease with a higher modulation index, thus, approaching 1 [25]. This could be seen in the high harmonic presence in the 400 Wm^{-2} compared to the 1000 Wm^{-2}. This implies that PV systems operating at comparably lower irradiation levels will inject higher harmonics into the grid because of the contrary relationship that exists between irradiation and harmonic distortion generation.

Figures 13 and 14 present the voltage harmonic distortions recorded for the 400 Wm^{-2} and 1000 Wm^{-2} scenarios. The individual harmonic distortions and the total harmonic distortions for both scenarios were within limits prescribed by the standards considered above. Distortions for both cases were similar in magnitude. The

Fig. 13 Voltage harmonic for 400 Wm^{-2}

THD = 2.24%

Fig. 14 Voltage harmonics for 1000 Wm^{-2}
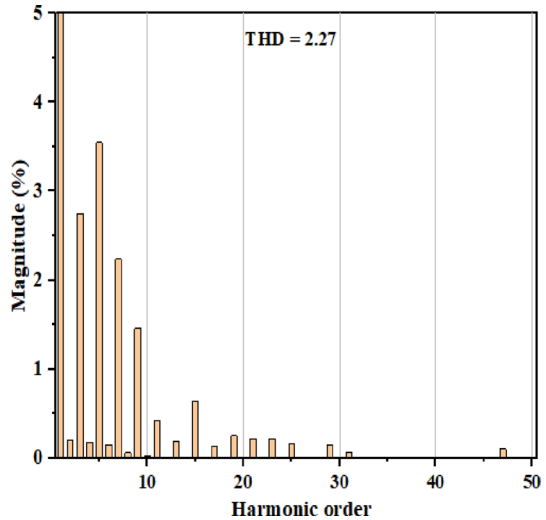
voltage total harmonic distortions were 2.24% and 2.27% respectively for 400 Wm^{-2} and 1000 Wm^{-2}, which were within limits prescribed by the standards. The 5th harmonics of both scenarios had total harmonic distortions of 3.545% and 3.47%, respectively, for 1000 Wm^{-2} and 400 Wm^{-2}. Apart from the 5th harmonics, all the other harmonics recorded distortions that were lower than 3% and within the limit of the standards for both cases under the solar simulator.

3.1.4 Frequency

The frequency profile plays a very critical role with regard to the power quality of the grid. A minimal deviation from the prescribed standards has a negative impact on the quality, stability, and reliability of the grid. Figure 15 presents the frequency
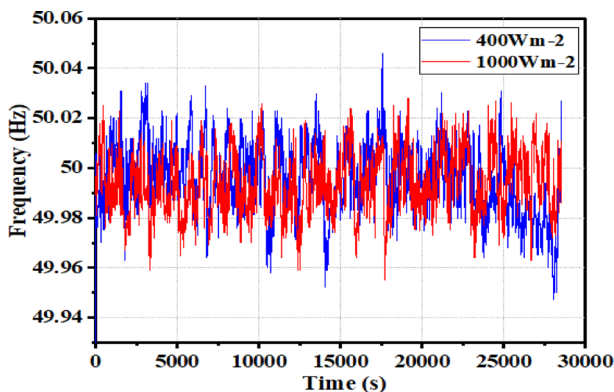
Fig. 15 Frequency profiles for the two scenarios of the solar simulator

profiles for the solar simulator application. The maximum and minimum frequencies for the 400 Wm^{-2} are 50.028 Hz and 49.955 Hz. The measured values did not present significant disparities, registering a standard deviation of 0.0125 Hz, indicating the nearness of the frequency during the entire period of experimentation with an average value of 49.994 Hz. The frequency evolution of 400 Wm^{-2} falls within the range of the standard by EN 50160 [21], which stipulates the frequency to be within ± 1% of the nominal frequency. The 1000 Wm^{-2} scenario recorded similar frequencies with the minimum and maximum frequencies being 49.629 Hz and 50.046 Hz, respectively. The average frequency and the standard deviations were 49.995 Hz and 0.017 Hz, respectively. The measured frequencies for the 1000 Wm^{-2} were within the acceptable range of ± 1% prescribed by EN 50160 [26].

3.1.5 Rapid voltage change

The Rapid Voltage Change (RVC), according to the IEC Standard 61000-4-30, defines RVC as a swift transition in the RMS voltage between two steady-state conditions, during which the voltage does not exceed the dip/swell thresholds [27]. Because the RVCs are events that occur suddenly, they are complicated to detect and track. Voltage events were recorded for both scenarios of 400 Wm^{-2} and the 1000 Wm^{-2}. The recorded events were all below the nominal velocity, as shown in Fig. 16. There were about twenty and eight voltage events for the 400 Wm^{-2} and the 1000 Wm^{-2}, respectively, as shown in Fig. 16a and b. The maximum and minimum voltage changes for the 400 Wm^{-2} were − 9.807 V and − 4.79 V, respectively. These changes lasted for 0.11 s and 0.01 s, respectively, for the maximum and minimum changes. The highest duration RVC lasted for 0.111 s and recorded voltage sags of − 8.65 V and − 7.893 V. With the case of the 1000 Wm^{-2}, the maximum and minimum RVC were − 9.828 V and − 5.481 V, respectively. These events lasted for 0.11 s and 0.01 s, respectively. The total duration for all the RVC recorded for the 1000 Wm^{-2} was 14 s, while it was 25.1 s for the 400 Wm^{-2} scenario. The most prolonged duration of the RVC for the 1000 Wm^{-2} was 0.12 s, and the voltage drop was − 8.308 V. According to

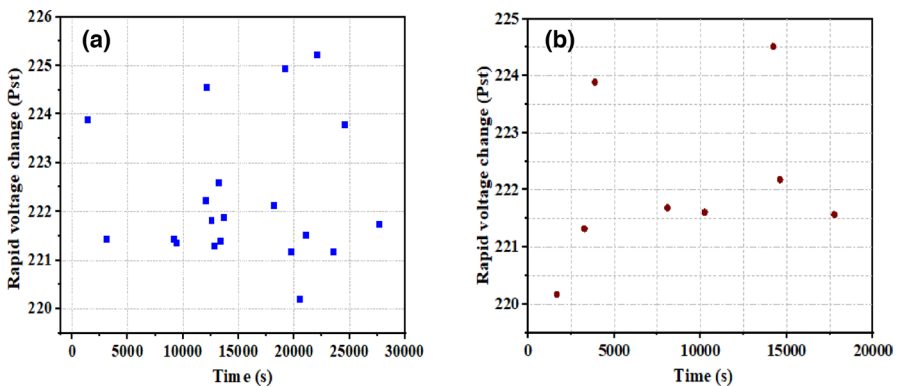**Fig. 16** Voltage events **a** 400 Wm^{-2} scenario, **b** 1000 Wm^{-2} scenario

[28], voltage deviations (sags and swells), rapid voltage changes (due to capacitor switching), harmonics and grounding were the most significant sources of power quality-related problems. With regards to RVC, the numerous events recorded by the 400 Wm^{-2} scenario show relatively higher issues of power quality compared with the higher constant irradiation generated by the solar simulator (1000 Wm^{-2}).

3.2 Power factor

The power factor (cos ϕ) (PF) shows the phase angle between the current and the voltage signals of the AC signal output. It is generally expressed as a decimal or in percentage. Per the IEEE 1547 standard, solar PV grid-connected inverters are to be designed to operate at a power factor close to unity. To maintain this characteristic, inverters are designed to suppress the reactive power to zero to achieve the abovementioned characteristic. The studied microinverter showed the same properties when the solar simulator was used. The technical regulations concerning power factor for most countries stipulate that the power factor range at the point of common coupling should be 0.95, whether leading or lagging [25]. Data were recorded at the time interval of 3 s. The maximum power factors were 0.99502 and 0.99627 for the 400 Wm^{-2} and 1000 Wm^{-2}, and the minimum values were 0.9 and 0.9213 for 400 Wm^{-2} and 1000 Wm^{-2}, respectively. The power factors throughout the study were almost all within the standard range of ≥ 0.95 except for four points within the study where the power factors were outside the prescribed scope, which may be the result of some losses. These occurred for both 400 Wm^{-2} and 1000 Wm^{-2}, but at different times, as shown in Fig. 17.
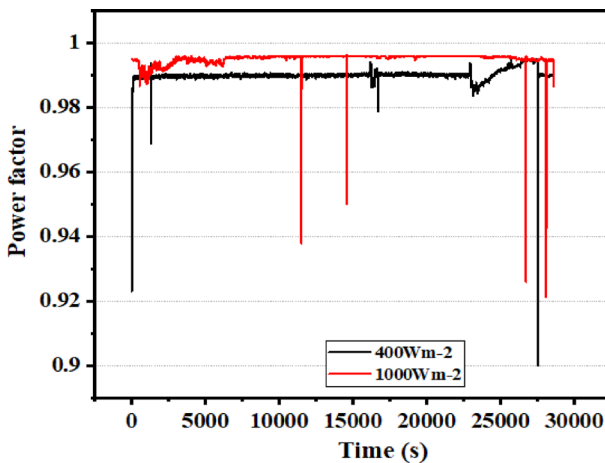

Fig. 17 Power factor for 400 Wm^{-2} and 1000 Wm^{-2}

3.3 Results and discussion for real modules under outdoor conditions

In this section, the results obtained from the measurements on the real modules under outdoor conditions are discussed, and comparisons made with the results obtained while using the solar PV simulator.

3.3.1 Frequency

Figure 16 presents the frequency profiles for the three different solar modules studied with the microinverter. The interval for measurement was 6 s. All the profiles obtained were within limits provided by the various standards, EN 50160 [21]. The three profiles showed similar trends, as seen in Fig. 18. The minimum, maximum and average values for all the cases showed no significant differences. This is evident in the standard deviation of 0.014005 Hz, 0.014324 Hz and 0.014175 Hz, respectively, for Solarex, Dunasolar and Juta modules. There was no significant difference between results under the solar simulator and those under the real outdoor operation.

The voltage profiles of the different technology solar PV modules studied under outdoor conditions using the microinverter are presented in Fig. 19. The voltage profiles observed under the studied modules were all within the prescribed voltage limits according to the various standards EN 50160, IEC 61000-4-6 [27, 29]. The voltage profiles for the Solarex module and the Juta module recorded voltages that were all above the nominal voltage of 230 V. The Dunasolar had voltage values of less than 1% that were below the nominal value of 300 V. The maximum values recorded were 237 V, 238 V, and 235 V for Solarex, Juta and Dunasolar, respectively. The minimum voltages were 231 V, 231 V and 225 V for Solarex, Juta and Dunasolar, respectively. The average voltages were 234.6 V, 235 V and 231.7 V, respectively, for the Solarex, Juta and Dunasolar modules. The glass-glass frameless module (Dunasolar) recorded the lowest range of voltage profile. The standard deviation was highest for the voltage profile of the Dunasolar (1.157 V) module compared to
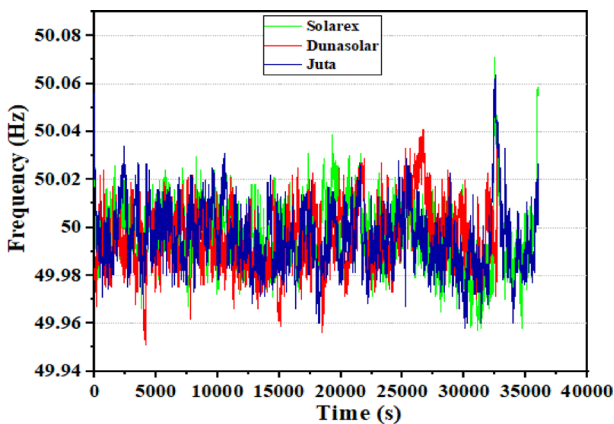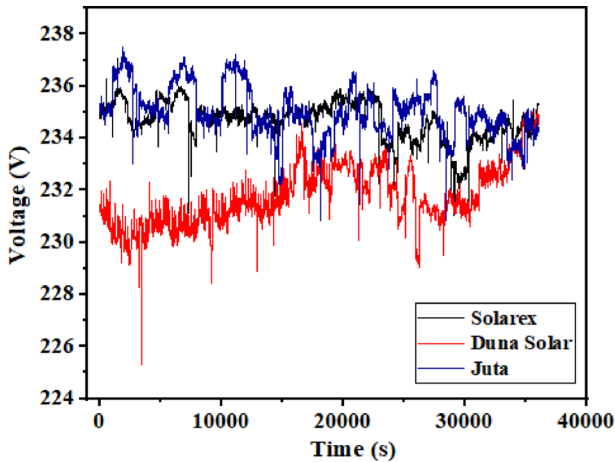

Fig. 18 Frequency profiles for Dunasolar, Solarex and Juta modules

Fig. 19 Voltage profiles for Dunasolar, Solarex and Juta modules

the pc-Si Solarex (0.727 V) and the mc-Si Juta modules (0.914 V). Comparing the voltage profiles recorded under the solar PV simulator with the results of the real modules in outdoor operation, the 400 Wm^{-2} under the solar simulator measurements had the highest voltage deviation, which was closely followed by the voltage profile of the Dunasolar module, even though both cases recorded a voltage variance of 10 V. The maximum voltages under both scenarios with the steady solar simulator were higher than all the studied cases with the real solar modules under outdoor operation. The deviations in the voltages recorded for the study under the solar simulator were higher than the standard deviations for the real solar modules under outdoor operation. However, both cases had the profiles within the limits set by the various standards.

3.3.2 Power factor

Figures 20, 21, and 22 present the power factor (PF) profiles for the different modules used under outdoor conditions to assess the performance of the micro-inverter. The power factor output depended significantly on the available irradiation as the power factor is derived from the values of the active power and the apparent power. This is an indication of the voltage and the current waveforms being out of phase. From the results, it can be seen that all three cases produced high percentages of values that were outside the limits prescribed by various standards for grid-connected solar PV systems, which should be 0.95, whether leading or lagging [25]. Except for the case of the Solarex modules, the power factors plunged into the negatives for the other cases with the lowest power factors reaching − 1.49 and − 1.33, respectively, for the Dunasolar and Juta modules. Comparing the outdoor scenarios to the study under the steady irradiation source of the solar simulator, the power factor profiles produced for all the cases studied using the solar simulator were all within the standard limits, while the
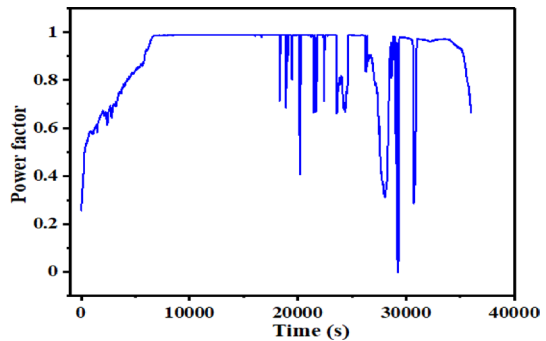
Fig. 20 Power factor profile for the Juta module study
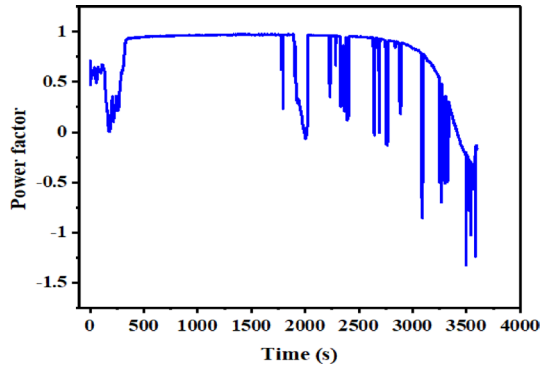
Fig. 21 Power factor profile for the Dunasolar module study
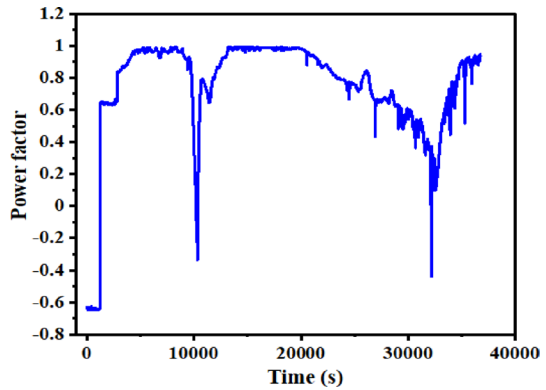
Fig. 22 Power factor profile for the Solarex module study

profiles for all the cases for the outdoor study had values that were outside the set limits. This points to the fact that unsteady solar radiation has a significant impact on the power factor profile. This is evident in the trend and correlation of the measured irradiation with the power factor profiles, as shown in Figs. 22 and 23 for the Solarex modules. The trend was similar for all three cases studied. The percentage of measured PF values that were below the standard limits for the
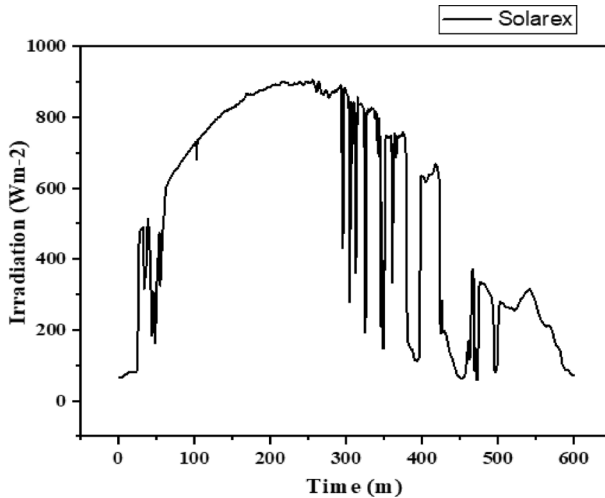
Fig. 23 Measured irradiation during the study with the Solarex module

cases studied are 67%, 54% and 37% for Dunasolar, Juta and Solarex modules, respectively.

3.3.3 Voltage events (rapid voltage change)

There were about 14 events occurring during the study with the Solarex module. The most prolonged duration of the RVC for the Solarex study was 0.13 s with a dip of − 11.212 V. The total time for the changes was 2.4 s. The minimal change was − 5.966 V, which lasted for 0.1 s. Results show that the study with the Juta module had the most voltage events of thirty-seven during the 10 h of experimentation, while the study with the Dunasolar recorded twenty RVC. The recorded RVC for the outdoor study were negative events and were within limits prescribed by the various standards (IEC 61000-4-30). The greatest RVC for the Juta study was − 11.32 V and had a duration of 0.04 s. The total time for the RVC for the investigation with the Juta module was 2.29 s. There were 20 RVCs for the Dunasolar study. The total time was 1.28 s, with the most significant change being − 11.32 V, which lasted for 0.04 s. In terms of power quality disturbances with regard to RVC, it can be said that the study with the Juta module had a high-power quality disturbance. The RVC for the study with Solarex modules, Dunasolar modules and Juta modules are presented in Figs. 24, 25 and 26, respectively.

The results for the voltage flicker for the study in outdoor conditions are shown in Figs. 27, 28 and 29. With reference to the standard for Pst at the PCC for grid-connected PV systems (EN 6100, IEEE 1547 and IEC 61000-3-3), Pst < 1.0 V and also between 0.6 and 0.9 pu for Plt and Pst, respectively [30]. The percentage of the recorded voltage flicker that fell outside the regulations for the various cases of the study was 2.5% for both the Juta and Solarex modules and 4% for the Dunasolar modules. The most severe of the recorded short-term flickers were 1.5, 1.6 and 2.9
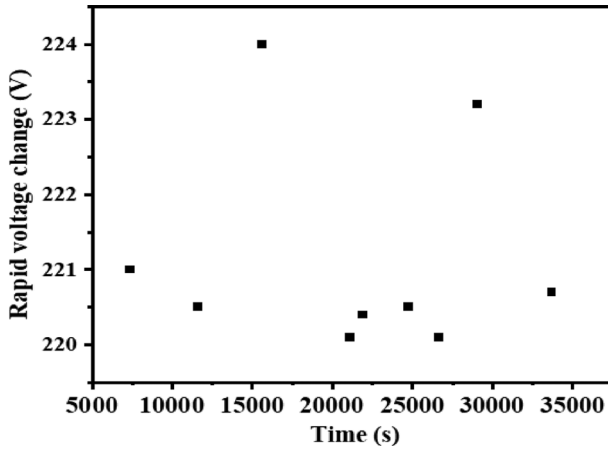
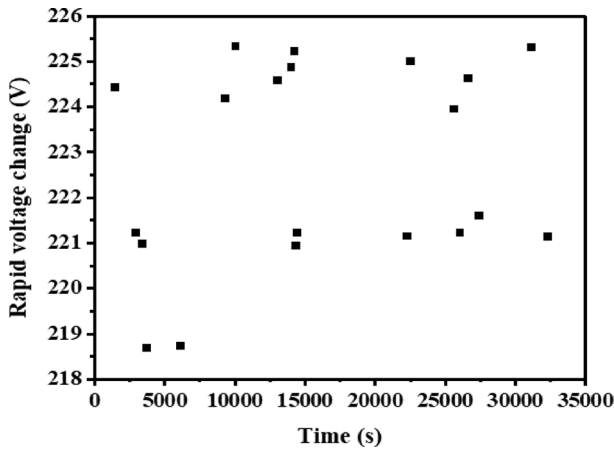**Fig. 24** RVC for the study with the Solarex modules

Fig. 25 RVC for the study with the Dunasolar modules

for the investigation with the Solarex module, Juta modules and the Dunasolar module, respectively. Studies have shown that the primary power quality issues caused by intermittent PV power generation are voltage fluctuation and light flicker [31, 32]. A study by [33] concluded the existence of a positive correlation between the PV system and flicker severity. They inferred that flicker values were as a result of the fluctuation of PV power output. Pakonen et al. [34] demonstrated that intermittent PV power production generates significant levels of short-term flicker values. An empirical study by Rahman et al. also revealed a minimal correlation between varying PV power generation and short-term flickers [35].

Comparing the results of the outdoor study with the results of the cases with the solar simulator, the percentage of the flickers of all three instances of the outdoor investigation that did not meet the standard requirements were all less than the
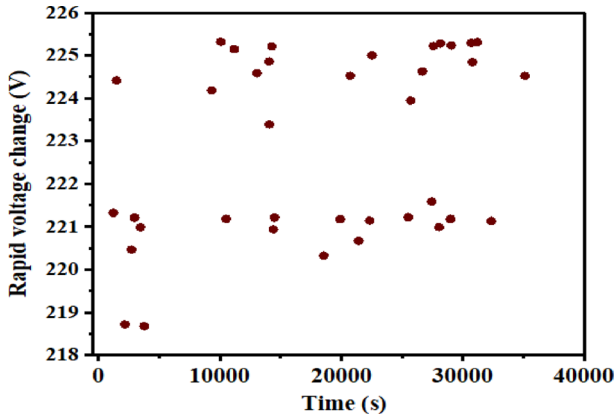
Fig. 26 RVC for the study with the Juta modules

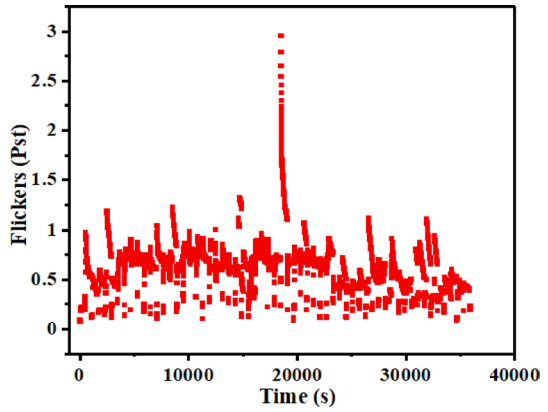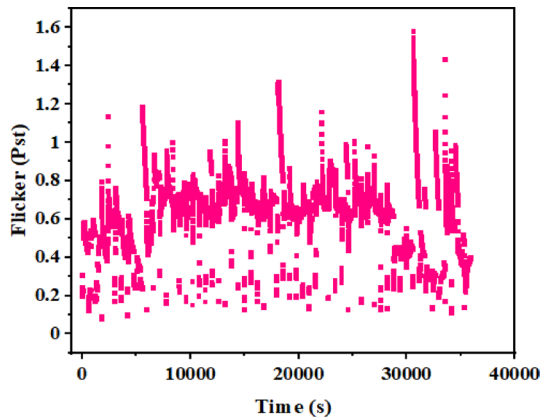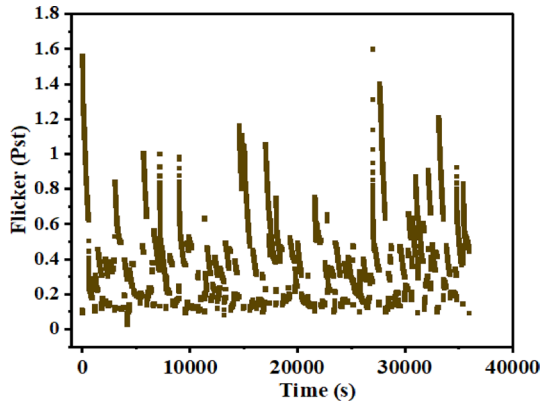**Fig. 27** Voltage flicker for Dunasolar modules

Fig. 28 Voltage flicker for Juta modules

Fig. 29 Voltage flicker for Solarex

results with the study with the solar simulator. Thus, the examination with the simulator had a higher severity of short-term flickers. It can be inferred that the intermittence of solar radiation (intermittent PV power generation) does not have a strong correlation with the measure of Pst in power output from the studied microinverter.
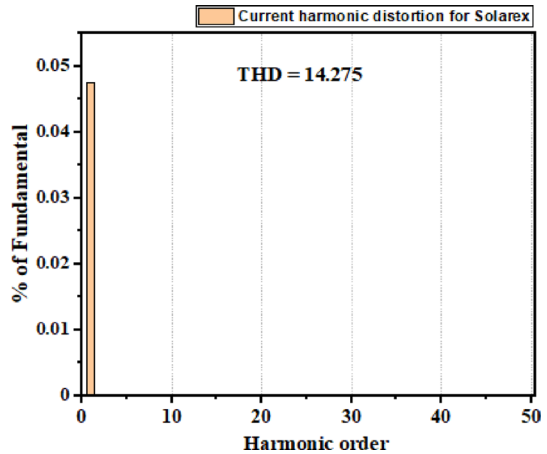
3.3.4 Harmonic distortions

Figures 30, 31 and 32 present the levels of harmonic distortions in the current output. Results reveal that the individual harmonic distortions for Juta, Dunasolar and Solarex scenarios were within the limit prescribed in IEEE 519 and the IEC 61000-3-2 standards. The individual harmonic distortions for all three cases were below 0.05%. However, the total harmonic distortions far exceeded the standard limit of 5% at the PCC for grid-connected PV systems. The THD for Juta, Dunasolar and Solarex were 27.43% and 33.6% and 14.275%. The study with the amorphous silicon glass module (Dunasolar) recorded the highest THD. It was evident that as the
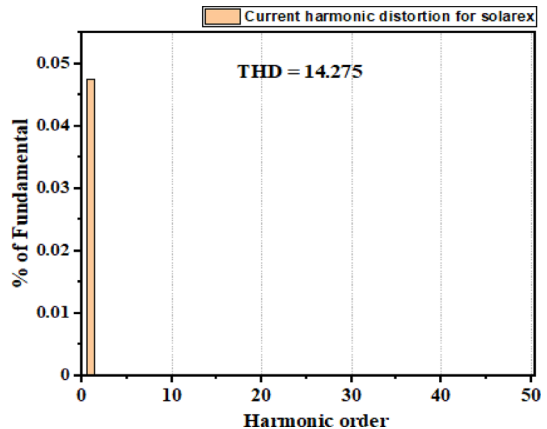

Fig. 30 Current harmonic distortions for the study with Juta modules
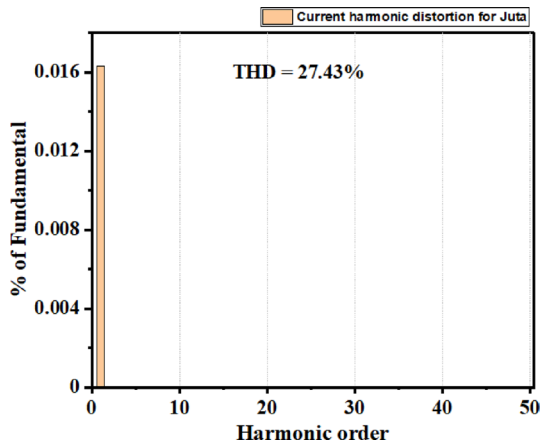
Fig. 31 Current harmonic distortions for the study with Dunasolar modules

Fig. 32 Current harmonic distortions for the study with Solarex modules

current increased, the THD increased for all cases studied. The level of the harmonic content of the output signal is dependent on the carrier frequency and the switching function. At low irradiation levels or increased temperatures, solar PV systems produce low fundamental components; consequently, increasing the generation of total harmonic distortions at fixed switching frequencies [36].

The results of the generated current THD for the studies with the solar simulator showed different trends compared to the results with the outdoor studies with the real solar modules, as presented in Fig. 33. It is seen that the THD output with the solar simulator (constant solar irradiation) was relatively steady with non-significant changes throughout the study. The THD generated in the outdoor study with the microinverter had their minimum values at the start of the study at 8 am. The trend, however, changed with time; it began to increase for all three cases, even though the values were different for all the cases. The increase in the output for the Solarex, however, had a drastic upward change at about half past noon, after which it continued to increase linearly with time until the end of the study. There was a strong
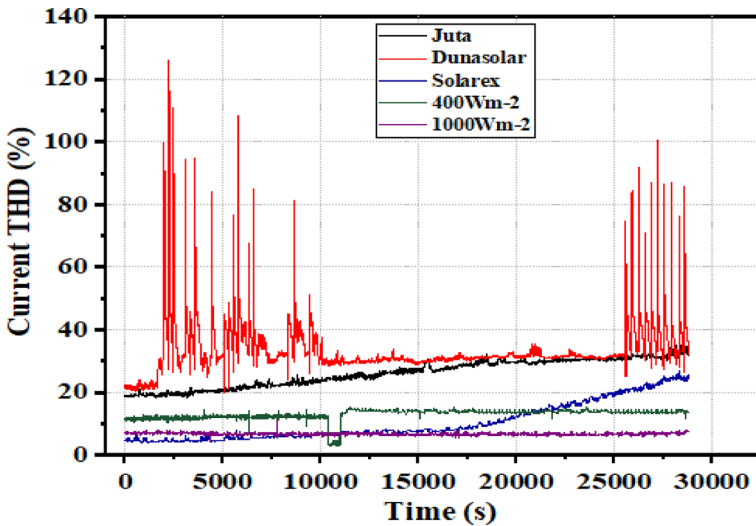
**Fig. 33** Current THD for the studies with Juta, Dunasolar and Solarex (400 Wm^{-2} and 1000 Wm^{-2})

correlation between the drastic change in the current THD of the Solarex module with the trend of irradiation for the day. It was apparent that at the time of change, there was an unsteady radiation incident at the site, as shown in Fig. 23, and this intermittence continued until the end of the experimentation. The THD output for the Solarex was also the least from the start of the investigation until the point of the drastic increase at about noon when it rose above the results for the solar simulator but not above the results for the other outdoor investigations. The trend for the Dunasolar (a-Si frameless glass solar module) rose continuously from its minimum value at the start of the study. It showed a unique behaviour during low unsteady or intermittent irradiation values. The THD increased enormously during such periods of irradiation, with values reaching as high as 126%. However, during periods of fairly steady solar irradiations, the generated THD for the Dunasolar was relatively stable.

The voltage harmonic contents for the outdoor measurements are presented in Figs. 34, 35 and 36. The individual harmonic distortions and the total harmonic distortions recorded for all the cases studied in the outdoor conditions were within limits stated by the standards (IEEE 519, IEC 61000-3-2), as shown in Table 3. The THDs were 1.94%, 1.97% and 2.03%, respectively, for Juta modules, Dunasolar module and Solarex modules. The 7th harmonic order for the Dunasolar module had distortions that were above 3% but less than 5%. The other individual harmonic distortions for Dunasolar were below 3%. The individual harmonic distortions for Juta modules were all below 3%. The 5th Harmonic order of the Solarex modules had distortions of 3.5%, apart from which the distortions for all the other harmonic orders were below 3%. It can be seen that the results (individual and total voltage harmonic distortions) for the outdoor study for all the scenarios were less than the values measured for the investigation with the steady

**Fig. 34** Voltage harmonic distortion for the study with Juta modules
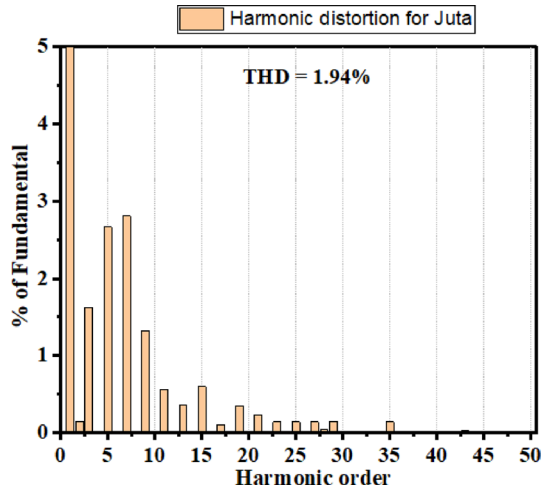
Fig. 35 Voltage harmonic distortion for the study with Dunasolar modules
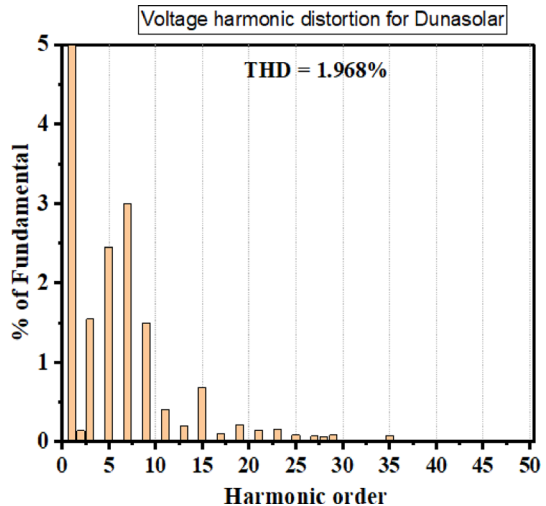
irradiation source (solar simulator). It can be inferred that the intermittency of solar radiation has no significant correlation with the voltage harmonic content recorded for all the cases studied.

Microinverters have the advantage of flexibility of use and high efficiency in maximum power point tracking because of their single-module converter applications. The studied microinverters operation in steady-state conditions showed outputs of power factor and current THD that were within acceptable standards. The microinverters' output under intermittent or transient power generation conditions was at variance with the grid standards. The solution, however, depends on the voltage regulator being able to control the effects of the transient/intermittent conditions by reducing the settling time under varying conditions and the

Fig. 36 Voltage harmonic distortion for Solarex modules
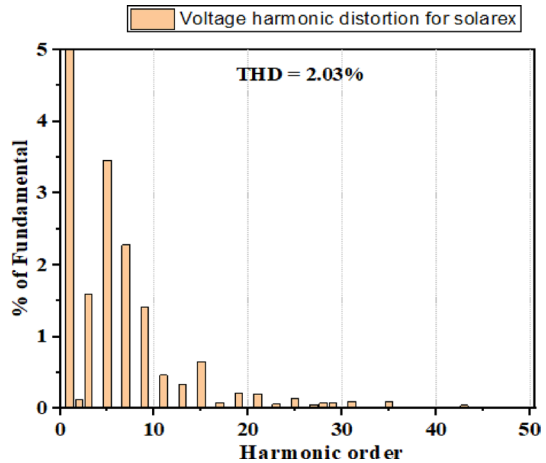
microinverter control characteristics [3]. In a low-power operating condition, the current THD effects of the microinverters far exceeded the acceptable standards.

Since the application of microinverters is concentrated in small-size PV systems, their effect on the grid output quality would be insignificant. However, as the microinverter systems are being disseminated and applied for large systems their effect could be significant on the grid performance.

Also, voltage fluctuations occur as a result of the rapid change in the rate at which different loads draw power or power is generated. In the instance of power generation, it occurs in power generators which are characterized by high levels of variability, e.g., solar PV systems. However, this study considered an environment with insignificant influence by local loads hence the output was significantly influenced by the inverter conversion characteristics and the set conditions.

4 Conclusions

Grid-connected inverters play a crucial role in feeding power from distributed sources into the grid. With the increasing growth of grid-tied solar PV systems (both rooftop and utility-scale) over the last decade, the awareness of power quality issues has risen with new power quality regulations and standards imposed by different countries and sub-regions to regulate power fed into the grid from distributed sources and hence ensure the stability of the power grid.

In this paper, the power quality analysis of microinverters has been presented. Power quality issues such as power factor, voltage flickers, current and voltage harmonics, voltage deviation, and voltage events with regard to compliance with standards and requirements for the integration of solar PV into the grid have been studied under a steady solar radiation source and real outdoor operation conditions.

Results show that the current THD measured for the studied microinverter under outdoor conditions far exceeded the current THD for the study with the PV simulator. However, the results of the voltage THD for the two studied cases showed the

reverse trend. There was a correlation between the intermittence of solar radiation and the current THD. The a-Si glass module exhibited this trend more significantly.

The voltage and current THD for the 400 Wm^{-2} and the 1000 Wm^{-2} scenarios under steady solar radiation were 2.24%, 13%, and 2.27, 6.93%, respectively. The voltage and current THDs for the outdoor study were 2.03% and 14.28% for Solarex (pc-Si module), 1.94% and 27.43% for Juta (mc-Si modules), and 1.97% and 33.6% for Dunasolar (a-Si glass module). Results showed that the intermittency of the radiation has a more significant influence on the magnitude of the harmonics than the intensity of the radiation. The voltage THD for all the studied cases were within the limits of the integration standards considered.

The measured power factors for the outdoor studies exhibited varying trends with compliance with the integration requirements. The percentage PF values outside (below) the standard limits for the cases studied were 67%, 54% and 37% for Dunasolar, Juta and Solarex modules, respectively. The PF for the studies under the PV simulator were almost 100% in conformity with the standards except for four and three values for 1000 Wm^{-2} and 400 Wm^{-2}, respectively, that fell below the standards.

Data availability The data supporting the findings of this study are available upon request from the corresponding author.

Declarations

Conflict of interest The authors declare that they do not have any conflict of interest.

References

1. Liu, W., Luo, F., Liu, Y., Ding, W.: Optimal siting and sizing of distributed generation based on improved nondominated sorting genetic algorithm II. Processes **7**, 1–10 (2019). https://doi.org/10.3390/PR7120955
2. Dixit, M., Kundu, P., Jariwala, H.R.: Integration of distributed generation for assessment of distribution system reliability considering power loss, voltage stability and voltage deviation. Energy Syst. **10**, 489–515 (2019). https://doi.org/10.1007/s12667-017-0248-6
3. Wu, A., Philpott, A., Zakeri, G.: Investment and generation optimization in electricity systems with intermittent supply. Energy Syst. **8**, 127–147 (2017). https://doi.org/10.1007/s12667-016-0210-z

4. Mancarella, P., Chicco, G.: Global and local emission impact assessment of distributed cogeneration systems with partial-load models. Appl. Energy **86**, 2096–2106 (2009). https://doi.org/10.1016/j.apenergy.2008.12.026

5. Energy manager. https://www.energymanagermagazine.co.uk/power-quality-issues-part-1-harmonics/ (2019). Accessed 15 Aug 21

6. Sher, H.A., Addoweesh, K.E.: Micro-inverters—promising solutions in solar photovoltaics. Energy Sustain. Dev. **16**, 389–400 (2012)

7. Petreuş, D., Daraban, S., Ciocan, I., Patarau, T., Morel, C., Machmoum, M.: Low cost single stage micro-inverter with MPPT for grid connected applications. Sol. Energy **92**, 241–255 (2013). https://doi.org/10.1016/j.solener.2013.03.016

8. Deline, C., Meydbray, J., Donovan, M.: Photovoltaic shading testbed for module-level power electronics: 2014 update. NREL Tech. Rep. NREL/TP-5200-57991. 32 (2012)

9. Myrzik, J.M.A., Calais, M.: String and module integrated inverters for single-phase grid connected photovoltaic systems—a review. In: 2003 IEEE Bologna PowerTech—Conference Proceedings, Bologna, Italy, pp. 8–15 (2003). https://doi.org/10.1109/ptc.2003.1304589

10 Kjaer, S.B., Pedersen, J.K., Blaabjerg, F.: A review of single-phase grid-connected inverters for photovoltaic modules. IEEE Trans. Ind. Appl. **41**, 1292–1306 (2005)

11. Kerekes, T., Teodorescu, R., Rodríguez, P., Vázquez, G., Aldabas, E.: A new high-efficiency single-phase transformerless PV inverter topology. IEEE Trans. Ind. Electron. **58**, 184–191 (2011). https://doi.org/10.1109/TIE.2009.2024092

12. Cavalcanti, M.C., De Oliveira, K.C., De Farias, A.M., Neves, F.A.S., Azevedo, G.M.S., Camboim, F.C.: Modulation techniques to eliminate leakage currents in transformerless three-phase photovoltaic systems. IEEE Trans. Ind. Electron. **57**, 1360–1368 (2010). https://doi.org/10.1109/TIE.2009.2029511

13. Islam, M., Mekhilef, S.: An improved transformerless grid connected photovoltaic inverter with reduced leakage current. Energy Convers. Manag. **88**, 854–862 (2014). https://doi.org/10.1016/j.enconman.2014.09.014

14 Khan, A., Ben-Brahim, L., Gastli, A., Benammar, M.: Review and simulation of leakage current in transformerless microinverters for PV applications. Renew. Sustain. Energy Rev. **74**, 1240–1256 (2017)

15. Araújo, S.V., Zacharias, P., Sahan, B.: Novel grid-connected non-isolated converters for photovoltaic systems with grounded generator. In: PESC Record—IEEE Annual Power Electronics Specialists Conference, Ixia/Rhodes, Greece, pp. 58–65 (2008). https://doi.org/10.1109/ptc.2003.1304589

16. Tang, Y., Yao, W., Loh, P.C., Blaabjerg, F.: Highly Reliable transformerless photovoltaic inverters with leakage current and pulsating power elimination. IEEE Trans. Ind. Electron. **63**, 1016–1026 (2016). https://doi.org/10.1109/TIE.2015.2477802

17. Kjaer, S.B., Pedersen, J.K., Blaabjerg, F.: Power inverter topologies for photovoltaic modules—a review. In: Conference Record—IAS Annual Meeting (IEEE Industry Applications Society), Pittsburgh, USA, pp. 782–788 (2002). https://doi.org/10.1109/ias.2002.1042648

18. Meinhardt, M., O'Donnell, T., Schneider, H., Flannery, J., O Mathuna, C., Zacharias, P., Krieger, T.: Miniaturized 'low profile' Module Integrated Converter for photovoltaic applications with integrated magnetic components. Conf. Proc. IEEE Appl. Power Electron. Conf. Expo. APEC, 1, Dallas, TX, USA, pp. 305–311 (1999). https://doi.org/10.1109/apec.1999.749656

19 Hossain, M.A., Xu, Y., Peshek, T.J., Ji, L., Abramson, A.R., French, R.H.: Microinverter thermal performance in the real-world: measurements and modeling. PLoS One (2015). https://doi.org/10.1371/journal.pone.0131279

20. Braun, M., Stetz, T., Bründlinger, R., Mayr, C., Ogimoto, K., Hatta, H., Kobayashi, H., Kroposki, B., Mather, B., Coddington, M., Lynn, K., Graditi, G., Woyte, A., MacGill, I.: Is the distribution grid ready to accept large-scale photovoltaic deployment? State of the art, progress, and future prospects. In: Progress in Photovoltaics: Research and Applications, 26th EU PVSEC Conference, Hamburg, Germany, pp. 681–697 (2012). https://doi.org/10.1002/pip.1204

21. CENELEC: En 50160. Eur. Stand. 1–20 (2007)

22. Ferdowsi, F., Mehraeen, S., Upton, G.B.: Assessing distribution network sensitivity to voltage rise and flicker under high penetration of behind-the-meter solar. Renew. Energy **152**, 1227–1240 (2020). https://doi.org/10.1016/j.renene.2019.12.124

23. Tagare, D.M.: Interconnecting distributed resources with electric power systems. In: Hanzo, L. (ed) Electric Power Generation. pp. 301–313. IEEE Press, New Jersey, USA (2011). https://doi.org/10.1002/9780470872659.ch15

24. Alexander, S.A.: Development of solar photovoltaic inverter with reduced harmonic distortions suitable for Indian sub-continent, (2016)

25 Al-Shetwi, A.Q., Hannan, M.A., Jern, K.P., Alkahtani, A.A., Abas, A.E.P.G.: Power quality assessment of grid-connected PV system in compliance with the recent integration requirements. Electronics (2020). https://doi.org/10.3390/electronics9020366

26 Dreidy, M., Mokhlis, H., Mekhilef, S.: Inertia response and frequency control techniques for renewable energy sources: a review. Renew. Sustain. Energy Rev. **69**, 144–155 (2017)

27. IEC Standard: IEC 61000-4-30 Corrigendum 1—ELECTROMAGNETIC COMPATIBILITY (EMC)—Part 3-40: testing and measurement techniques—Power quality measurement methods. IEC Stand. Corrigendum 1. 2016–2017 (2015)

28. Melhom, C.J., Maitra, A., Sunderman, W., Waclawiak, M., Sundaram, A.: Distribution system power quality assessment phase II: voltage sag and interruption analysis. In: Record of Conference Papers—Annual Petroleum and Chemical Industry Conference, pp. 113–120 (2005)

29. Markiewicz, H., Klajn, A.: Voltage disturbances Standard EN 50160—voltage characteristics in public distribution systems (2004)

30. Basso, T., Chakraborty, S., Hoke, A., Coddington, M.: IEEE 1547 Standards advancing grid modernization. In: 2015 IEEE 42nd Photovoltaic Specialist Conference, PVSC 2015 (2015)

31 Shivashankar, S., Mekhilef, S., Mokhlis, H., Karimi, M.: Mitigating methods of power fluctuation of photovoltaic (PV) sources—a review. Renew. Sustain. Energy Rev. **59**, 1170–1184 (2016)

32. Zhao, K., Ciufo, P., Perera, S.: Rectifier capacitor filter stress analysis when subject to regular voltage fluctuations. IEEE Trans. Power Electron. **28**, 3627–3635 (2013). https://doi.org/10.1109/TPEL.2012.2228279

33. Lim, Y.S., Tang, J.H.: Experimental study on flicker emissions by photovoltaic systems on highly cloudy region: a case study in Malaysia. Renew. Energy **64**, 61–70 (2014). https://doi.org/10.1016/j.renene.2013.10.043

34. Pakonen, P., Hilden, A., Suntio, T., Verho, P.: Grid-connected PV power plant induced power quality problems—experimental evidence. 2016 18th Eur. Conf. Power Electron. Appl. EPE 2016 ECCE Eur., Karlsruhe, Germany, pp. 1–10 (2016). https://doi.org/10.1109/EPE.2016.7695656

35. Rahman, S., Moghaddami, M., Sarwat, A.I., Olowu, T., Jafaritalarposhti, M.: Flicker estimation associated with PV integrated distribution network. In: Conference Proceedings—IEEE Southeastcon, St. Petersburg, FL, USA, pp. 1–6 (2018). https://doi.org/10.1109/SECON.2018.8479058

36. Jadeja, R., Ved, A.D., Chauhan, S.K., Trivedi, T.: A random carrier frequency PWM technique with a narrowband for a grid-connected solar inverter. Electr. Eng.. Eng. **102**, 1755–1767 (2020). https://doi.org/10.1007/s00202-020-00989-6